Supplementary Figures

High Loading of Transition Metal Single Atoms on Chalcogenide Catalysts

Jianwei Zheng,[1] Konstantin Lebedev,[1] Simson Wu,[1] Chen Huang,[2] Tuğçe Ayvalı,[1] Tai-Sing Wu,[3] Yiyang Li,[1] Ping-Luen Ho,[1] Yun-Liang Soo,[3] Angus Kirkland,[2] and Shik Chi Edman Tsang[1]*

[1]Wolfson Catalysis Centre, Department of Chemistry, University of Oxford, Oxford, OX1 3QR, UK.

[2] Department of Materials, University of Oxford, Oxford, OX1 PH, UK

[3]Department of Physics, National Tsing Hua University, Hsinchu, Taiwan.

Correspondence and requests for materials should be addressed to S.C.E.T. (email: edman.tsang@chem.ox.ac.uk).

Table of Contents

Experimental

Chemicals. MoS_2 (Sigma-Aldrich); WS_2 (99%, Sigma-Aldrich); WSe_2 (99.8%, Alfa Aesar); $MoSe_2$ (99.9%, Alfa Aesar); Fe acetate (reagent grade, Alfa Aesar); $FeCl_3 \cdot 6H_2O$ (reagent grade, Alfa Aesar); $FeCl_2$ (reagent grade, Sigma-Aldrich); n-butyllithium/hexane (1.6M, Sigma-Aldrich); Polyvinylpyrrolidone (PVP, reagent grade, Sigma-Aldrich); Isopropanol (99.9%, Sigma-Aldrich); HCl (≥ 98%, Sigma-Aldrich); Hydrazine monohydrate (98%, Sigma-Aldrich); Thiophene (≥ 99%, Sigma-Aldrich); Platinum (II) bis(acetylacetonate) (97%, Sigma-Aldrich); Ru acetylacetonate (97%, Sigma-Aldrich); Cu acetate (reagent grade, Sigma-Aldrich); Co acetate (reagent grade, Sigma-Aldrich); Ni acetate (reagent grade, Sigma-Aldrich); FeS (reagent grade, Sigma-Aldrich); Pd acetate (98%, Sigma-Aldrich).

Catalyst preparation. 2D chalcogenide materials (MoS_2, $MoSe_2$, WS_2 and WSe_2) were exfoliated to monolayers based on a previously reported chemical method. MoS_2 powder was also exfoliated by using hydrazine.[1] The resultant 2D materials were then dispersed in water/isopropanol (1:3, v/v) mixture in the presence of 30 mg of PVP. After sonicating for 1h, these 2D materials maintained a colloidal state without restacking. A modified hydrothermal method was used to load various TMs on these exfoliated 2D materials. In a typical experiment, 0.2 mM of the desired transition metal precursor was dissolved in 1 mL of 0.5 mM thiourea solution and kept overnight to form the relevant urea coordinated TM complex. Subsequently, the TM complex was introduced to a specific amount of colloidal 2D material dependent on the loading required. The mixture was then transferred to an autoclave and heated at 160 °C for 16h. After cooling, the precipitate was washed with deionized water and dried under vacuum for 12h to obtain the final solid product. The resultant solid was then reduced in a flow of $5\%H_2/N_2$ (40 mL/min) for 2h to yield TM doped single layer chalcogenide. Similar procedure was used to prepare Fe-MoS_2-nt without using thiourea and Fe-$_N$$MoS_2$ when using hydrazine exfoliated MoS_2.

Characterization. Transition metal loading was analysed by ICP-OES using an Optima2100DV, PerkinElmer. Microwave acid digestion and ICP-mass spectroscopy (MS) analyses were also employed to double check the loading using an Agilent 7800 ICP-MS in East Anatolia High Technical Application and Research Centre at Ataturk University, Turkey. Continuous-wave EPR spectra were acquired using an X-band (9.4 GHz) Bruker EMX EPR spectrometer. Then X-Band spectra were performed over a 300 Gauss field range and 15 scans were collected. XRD patterns were obtained using a Bruker AXS D5005 diffractometer operating at 30 mA and 40 kV (scan rate 0.000267°/s, step size at 0.004°, time per step at 15 s, total number of steps at 15000). Samples were ground and pressed onto a glass plate for XRD analysis. TEM samples were prepared by grinding and then dispersing solid material in isopropanol by sonication. The solution was then drop cast onto a holey carbon coated 400 mesh Cu-TEM grid and dried at room temperature.

High-resolution scanning transmission electron microscopy (STEM) annular dark field (ADF) images were obtained using a probe corrected JEOL ARM300F at the electron Physical Sciences Imaging Centre at Diamond Light Source operated at 60 kV to avoid electron beam damage, with ADF inner and outer detector angles of 215.8 mrad, respectively and a 22.6 mrad convergence semi-angle. Prior to recording images, the sample was beam showered at 649 pA for 0.5-1 h to reduce contamination.

XPS spectra were acquired on a Quantum 2000 Scanning ESCA Microprob spectrometer (Harwell) with a Al K_α X-ray radiation source ($h\nu$ = 1486.6 eV). The sample was firstly pressed into a thin disc, and was reduced at 5% H_2–95% N_2 at 300 °C for 2 h. Binding energies were calibrated using the C 1s peak at 284.5 eV as reference; experimental errors were within ±0.2 eV. CasaXPS was used to calculate the compositions. PDF was carried out at Beamline I15, Diamond Light Source, Harwell, UK. Scattering data was collected at relatively high scattering angles using high energy powder diffraction and Fourier transformed to produce the PDF data. TOPAS was employed to simulate the spectra and the R factor was within 2%. Simulations of

the XANES spectra were performed in JFEFF. A 9.0. A (2×2) supercell of 2H-MoS_2 with a Fe atom /Fe_2 cluster /Fe_3 cluster atop Mo site was selected to simulate Fe-sMoS_2. The models were optimised by first principle DFT calculations using Vienna Ab-initio simulating package (VASP). A 15 Å region of vacuum in the *z*-direction was applied to separate the neighboring single-layered MoS_2 sheets. The Brillouin zone was sampled with an 8×8×4 and a 2×2×1 Monkhorst-Pack grid of k-points for geometry optimizations, respectively. TM K-edge and L-edge X-ray absorption spectra were collected in fluorescence mode at the BL07A XAS beamline of the NSRRC, Taiwan. To examine the local chemical environment of the TM atoms, EXAFS data were extracted from the XAS spectra. The Demeter Athena program was adopted for XAFS data analysis, where the data were calibrated, normalised and Fourier transformed. The least-squares curve fitting analysis of the EXAFS $\chi(k)$ data was carried out using the Demeter Artemis program. The EXAFS Wavelet was obtained on basis of this protocol and used calculations developed by Marina Chukalina and Harald Funke, The backscatter atoms in this method are within the same atomic shell. The spectra were calibrated with Fe foil and other Fe salts as references. The amplitude reduction factor was obtained from analysis of the Fe foil and used as a fixed input parameter for the refinement of the coordination number and bond distance of the absorption element. The decision as to which components correspond to noise and which are the signal related principle components (PCs) was made on the basis of the F-test of the variance associated with the jth PC and the summed variances associated with the noise components. The number of PCs having a % significance level located less than a test level of 5% were generally used. Qualitative analysis of the PCs was extracted by Singular Value Decomposition (SVD) of the XAS data matrix.

Operando DRIFTS experiments were conducted in a reaction chamber (HVC-DRP, Harrick) mounted with a Praying Mantis (Harrick) DRIFTS optical system. The UV−vis spectroscopic cell allows catalyst to be characterized under reaction conditions. The spectra were collected on a Nicolet 6700 apparatus equipped with a mercury cadmium telluride (MCT) detector at 300 °C, ambient pressure. Approximately 50 mg of catalyst was placed in the cell for each measurement. The flow of gases was controlled by means of mass flow controllers (Bronkhorst). Prior to each measurement, the catalyst was pretreated in situ at 300 °C in diluted H_2 for 2 h. The gases pass through the sample packed bed. Afterwards, a mixed flow of 25%CO_2 and 75%H_2 was flowed through the sample. The IR spectra were collected every minute to follow the reaction of the surface species.

CO_2-TPD was carried out in a quartz glass tube reactor with a TCD detector. 50 mg of sample was loaded in the glass reactor by quartz wool. Temperature was monitored by a K-type thermocouple at the sample. The sample was firstly pre-treated at 5% H_2 in N_2 (50 ml/min) at 300 °C for 2 h and was then cooled to 30 °C in flowing He, followed with a CO_2 flow (50 ml/min) for 30 minutes. Afterwards, the sample was purged with He to remove gas phase and weakly adsorbed species. Finally, TPD was started with 10 °C/min in He flow (50 ml/min).

For DFT calculations, we have performed a comprehensive analysis of transition metal doping at MoS_2 surfaces in terms of structures, energetics and hydrogen adsorption characteristics in view of understanding the factors that affect the reverse water gas shift reaction. A (2×2) supercell of 2H-MoS_2 with a Fe atom /Fe_2 cluster /Fe_3 cluster atop Mo site was selected to simulate Fe-sMoS_2. The models were optimised by first principle DFT calculations using Vienna Ab-initio simulating package (VASP) with the projector-augmented wave pseudopotential (PAW).[2,3] A 15 Å region of vacuum in the *z*-direction was applied to separate the neighboring single-layered MoS_2 sheets. The Brillouin zone was sampled with an 8×8×4 and a 2×2×1 Monkhorst-Pack grid of k-points for geometry optimizations, respectively. The generalized gradient approximation (GGA)[2] in the Perdew−Burke−Ernzerhof (PBE)[4] form was adopted and plane wave basis set were controlled with a cutoff energy of 450 eV. The limit for the ionic convergence and the electronic convergence was set to 0.02 eV $Å^{-1}$ and 10^{-5} eV, respectively.

The adsorption energies (Eads) onto the Fe_n/MoS_2 system are calculated as

$$Eads = E_{Mol/Cat} - E_{Cat} - E_{Mol}$$

where $E_{Mol/Cat}$, E_{Cat}, E_{Mol} are the energies of the molecule adsorbed on Fe_1/2H-MoS_2 system, Fe_1/2H-MoS_2 single layer, and isolate adsorbed molecule, respectively. The Gibbs free energy change (ΔG) of every elemental step was calculated. Free energy corrections to the electronic energy were calculated based on the standard vibrational corrections in the harmonic approximation to the enthalpy and entropy:

$$\Delta G = \Delta E + \Delta ZPE - T\Delta S + \Delta GU$$

where ΔE is the electronic energy difference, ΔZPE is the zero-point energy, T is set at 298.15 K, ΔS is the entropy change, and ΔGU is the free energy contributions related to the applied potential U (U = 0 was adopted in this study).

The effect of the electric field is much smaller than typical error estimates associated with DFT/GGA calculation hence it is neglectable. Notably, the zero-point energies and entropies of these intermediate species for RWGS were obtained by using the standard vibrational frequencies, in which the catalyst is fixed and the free-energy corrections to gas H_2, H_2O, OH, CO and CO_2 are taken from the NIST database (http://cccbdb.nist.gov/).

Catalytic performance test. A continuous flow reactor was built with a computer-controlled auto sampling system to evaluate the activity of catalysts for CO_2 hydrogenation. Typically, 100 mg of catalyst precursor was sandwiched between two beds of quartz wool at the center of the reactor. The catalyst precursors were firstly reduced at 573 K for 2 h in 5% H_2–95% N_2 and then cooled to the reaction temperature. The ratio of H_2/CO_2 was set to 3.0 in the feed gas and the pressure was held at 10 bar. The gas hourly space velocity (GHSV) was controlled at 9000 mL/g/h. The outlet stream was sampled in a loop in an automatic Valco 6-ports valve system and analysed using an on-line gas chromatograph (Agilent, 7890B). Sulfur tolerance test was evaluated by flowing the reactant gas through thiophene. The concentration of thiourea in gas mixture (~100 ppm) was controlled by a cooling bath of dry ice and acetone.

Results and Discussion

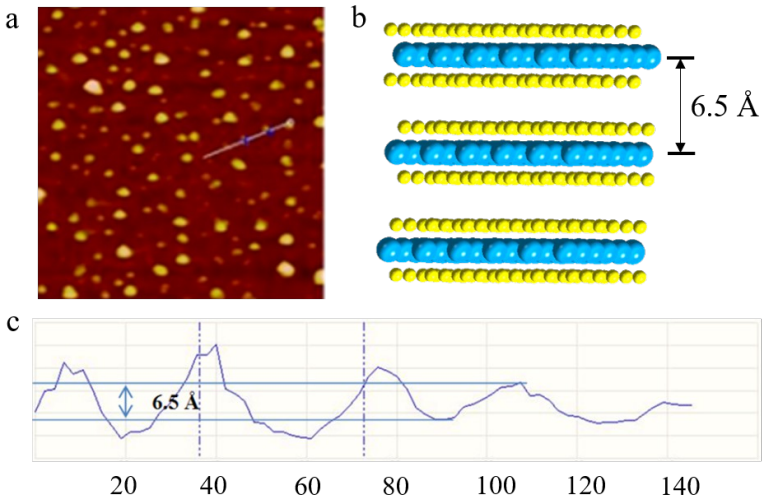

Figure S1. Atomic force microscopy (AFM) image analyses for chemically exfoliated $sMoS_2$. (a) AFM image of spin-coated $sMoS_2$ with a scan line. (b) Model of 2-H MoS_2 with 3-layer structure perpendicular to the c axis. (c) Line intensity profile along the line marked in a. Reprinted in part with permission from [1] Copyright 2017 Nature Publishing Group.

It can be seen that the step heights of the thinnest layers is 0.6-0.7 nm. This value is comparable to the thickness (ca. 0.65 nm) of a single layer of the S-Mo-S building block as shown in b. Statistical analysis of 100 flakes produced by the lithium exfoliation method revealed that 56% of the flakes were monolayers, 28% bilayers and 13% formed three layers or greater in dried form (mainly monolayers in solution). The line intensity profile indicates 4 MoS_2 species with 2, 3, 2, 1 layer of the S-Mo-S building block, respectively (see reference 28 in the main text).

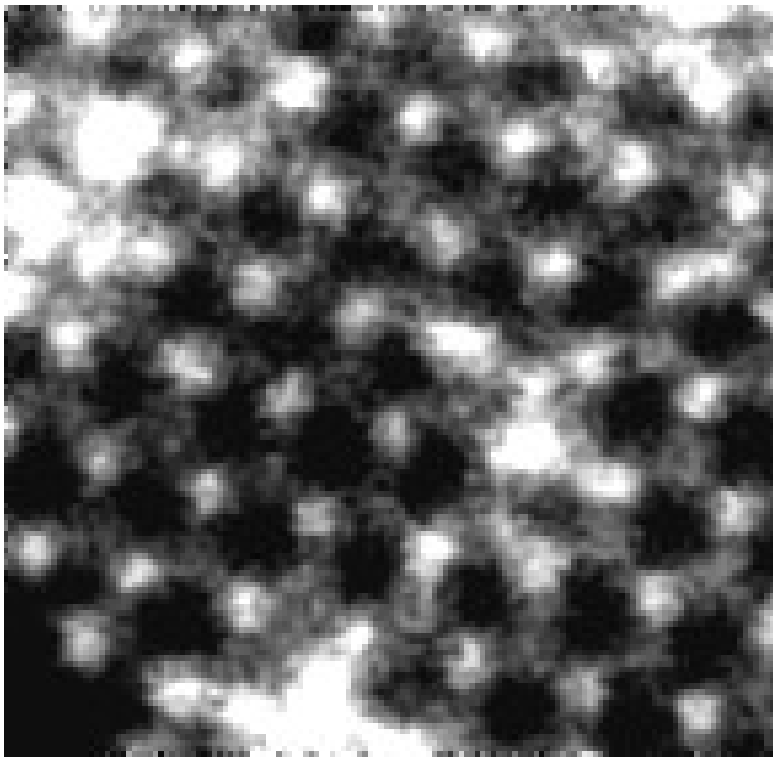

Figure S2. **a.** AC HAADF–STEM image of 3%Fe–sMoS_2. Scale bar, 0.5 nm. **b.** EELS recorded at the position marked in (a). The *L*3,2 edges for Fe are indicated.

Figure S3. Fe *k*-edge XANES spectra of atomically dispersed 10%Fe-sMoS_2. Fe foil, FeS, hydrated $FeCl_2$, and $FeCl_3$ were used as references.

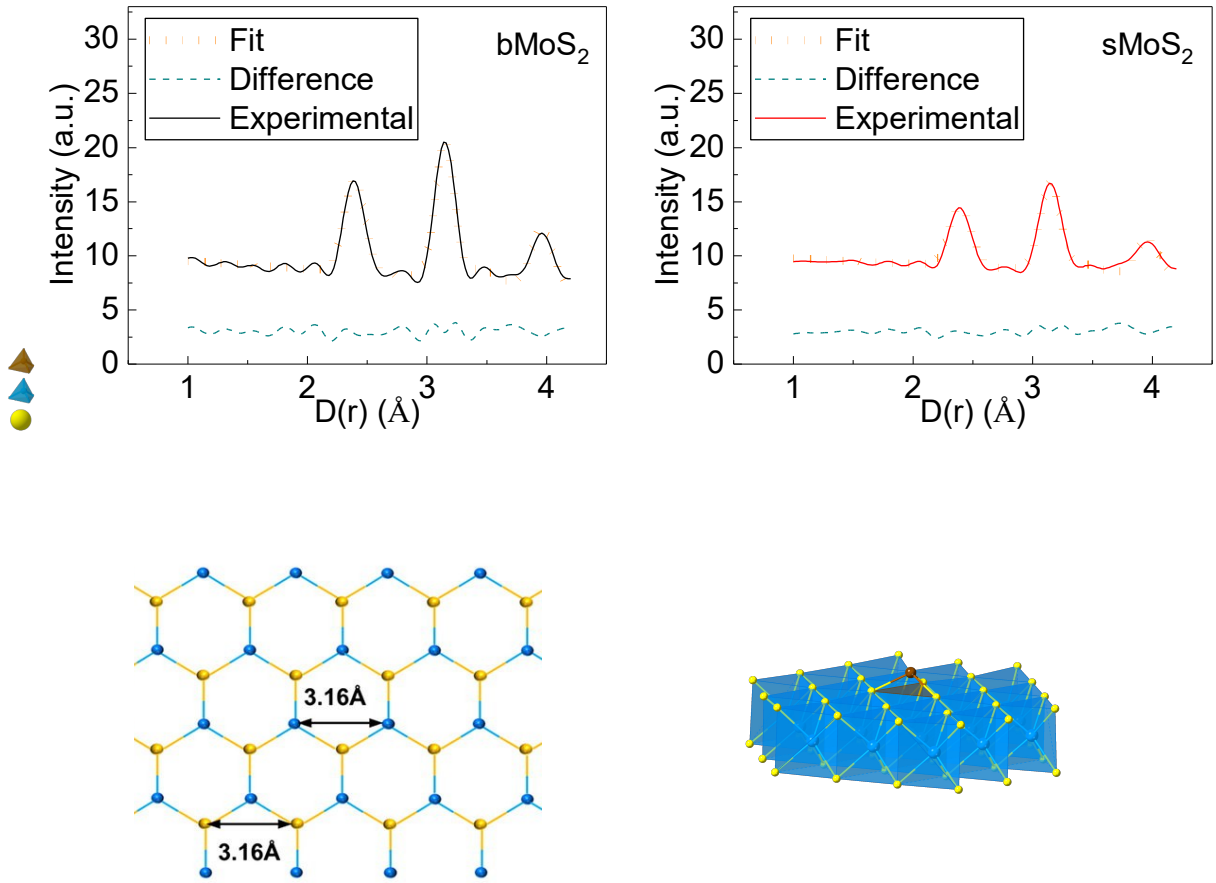

Figure S4. a. PDF spectra of $bMoS_2$, $sMoS_2$ and 3%Fe-$sMoS_2$. **b-d.** PDF and simulated spectra of $bMoS_2$, $sMoS_2$ and Fe-$sMoS_2$ respectively. **e.** Structure of $sMoS_2$. **f.** Fe-$sMoS_2$ structure as simulated shown in 3d. The three peaks at 2.38 Å, 3.15 Å, and 3.96Å in (b), (c) and (d) are attributed to Mo-S, Mo-Mo, and S-Mo bonds as indicated in €.

Figure S5. k^3-weighted *R*-space Fourier transform spectra of EXAFS for a) Fe-$sMoS_2$ and Fe-$sMoS_2$ (10 wt%) prepared without thiourea or PVP; b) Fe-$_N$$MoS_2$ and Fe-MoS_2 -nt.

Figure S6. TGA spectra for Fe-sMoS_2 precusor and as-reduced Fe-sMoS_2 (10 wt%).

Figure S7. IR spectra for Fe-sMoS$_2$ precusor and as-reduced Fe-sMoS$_2$ (10 wt%).

Figure S8. X-ray diffraction (XRD) patterns of $sMoS_2$ supported transition metals (10 wt%). The weak reflection observed at 15° is due to the restacking of $sMoS_2$. The broad peak at 26° is attributed to the amorphous silica of the glass plate.

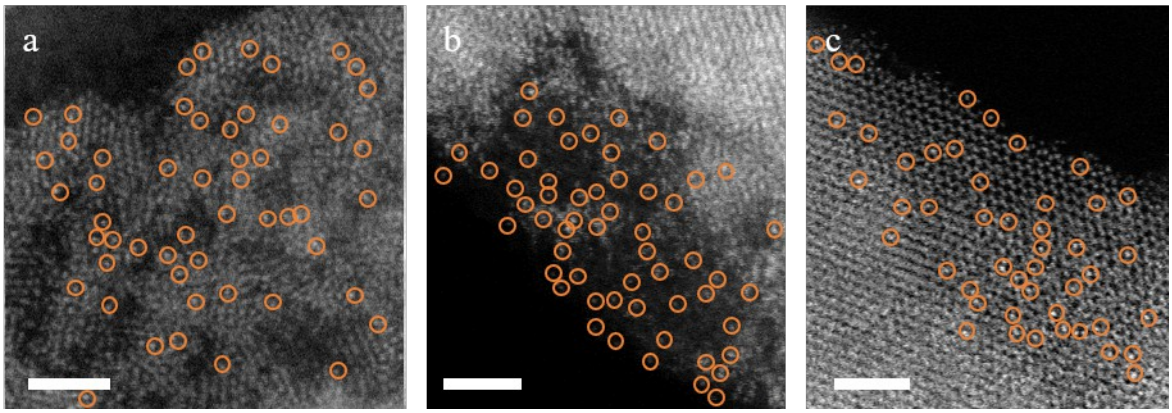

Figure S9. AC HAADF-STEM images for **a.** Pd-sMoSe$_2$, **b.** Pd-sWSe$_2$, and **c.** Pd-sWS$_2$. Pd loading, 10 wt%. Scale bars are, 2 nm in all cases. Pd SAs are circled.

Figure S10. X-ray diffraction (XRD) patterns of Fe-sMoS_2 with different weight loading.

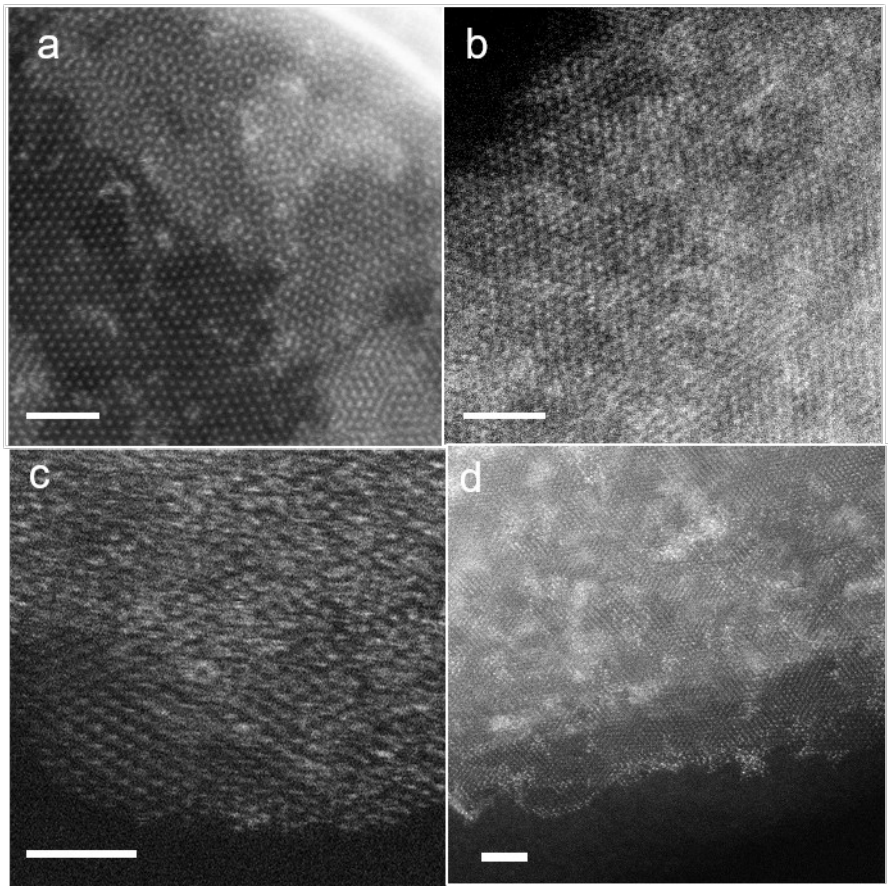

Figure S11. AC HAADF-STEM images of Fe-sMoS_2 with a Fe weight loading of **a.** 3%, **b.** 5%, **c.** 15% and **d.** 20%. Scale bar for all images is 2 nm.

Figure S12. Fe k-edge XANES spectra of atomically dispersed Fe-sMoS_2 with progressive addition of Fe (3-20 wt %). FeS, Fe foil, hydrated $FeCl_2$, and $FeCl_3$ were used as references.

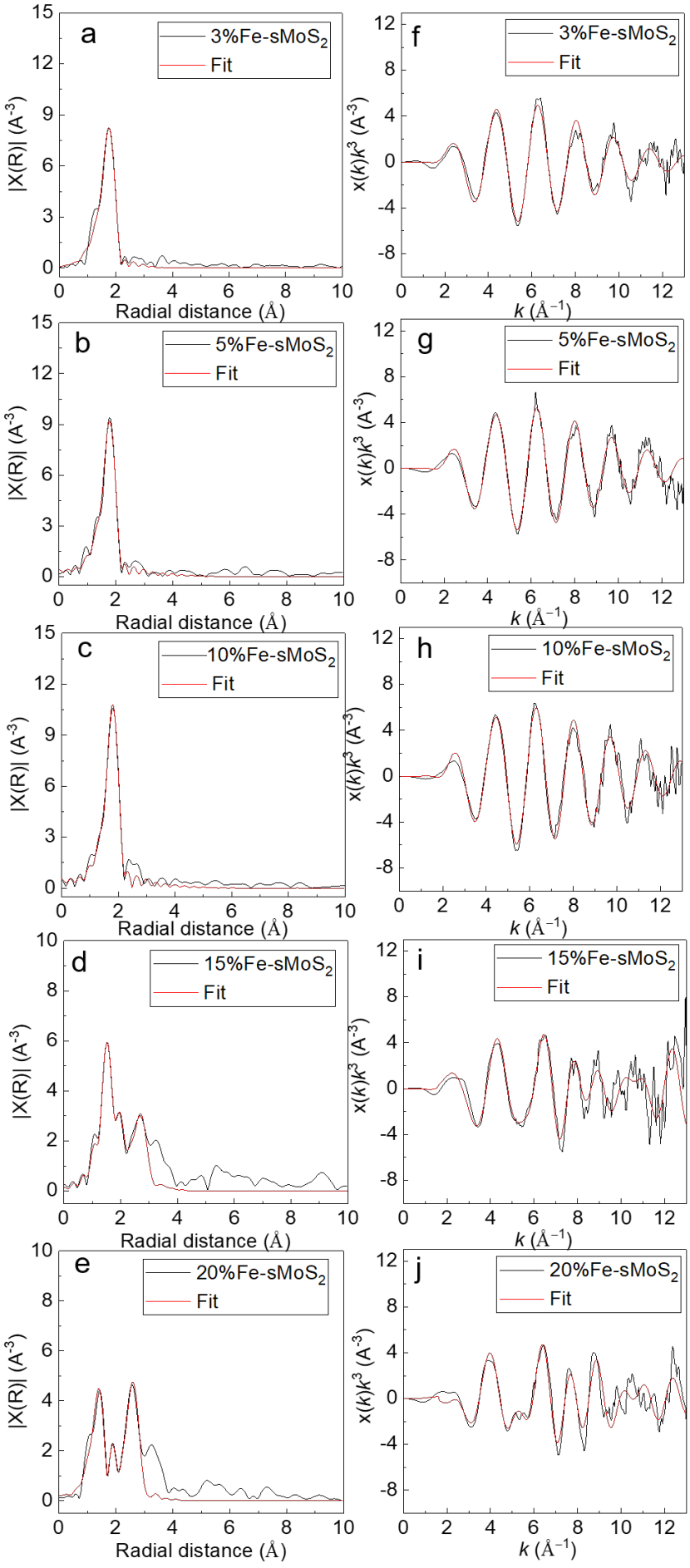
a
3%Fe-sMoS2
Fit
|X(R)| (A-3)
Radial distance (Å)
f
3%Fe-sMoS2
Fit
x(k)k3 (A-3)
k (Å-1)
b
5%Fe-sMoS2
Fit
|X(R)| (A-3)
Radial distance (Å)
g
5%Fe-sMoS2
Fit
x(k)k3 (A-3)
k (Å-1)
c
10%Fe-sMoS2
Fit
|X(R)| (A-3)
Radial distance (Å)
h
10%Fe-sMoS2
Fit
x(k)k3 (A-3)
k (Å-1)
d
15%Fe-sMoS2
Fit
|X(R)| (A-3)
Radial distance (Å)
i
15%Fe-sMoS2
Fit
x(k)k3 (A-3)
k (Å-1)
e
20%Fe-sMoS2
Fit
|X(R)| (A-3)
Radial distance (Å)
j
20%Fe-sMoS2
Fit
x(k)k3 (A-3)
k (Å-1)

Figure S13. a-e. k^3-weighted *R*-space Fourier transform and **f-j.** *k*-space EXAFS spectra with fits for for Fe-sMoS_2 at Fe weight loadings of 3-20%.

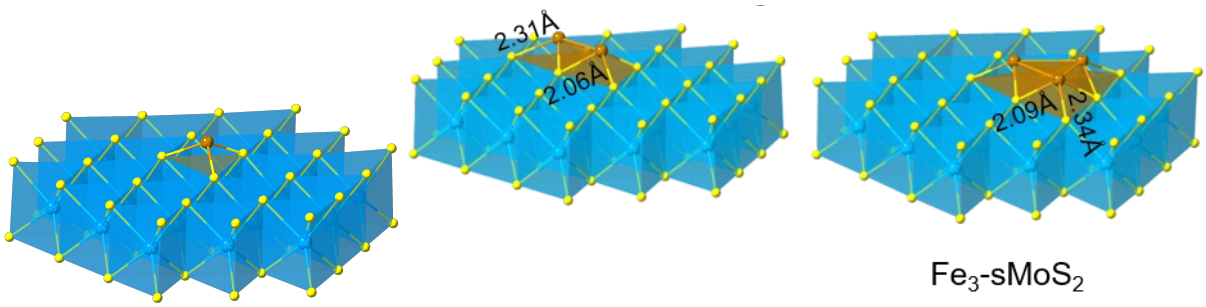

Figure S14. Optimised DFT models for Fe_1, Fe_2 and Fe_3 supported on $sMoS_2$. Values show the shortest and longest Fe-S bond distances in the first shell around Fe.

Figure 15. a. k^3-weighted *R*-space Fourier transform spectra of EXAFS and **b.** Pre-edge of Mo *k* -edge XANES spectra for $bMoS_2$, $sMoS_2$ and Fe-$sMoS_2$.

Figure S16. XPS spectra from Mo3d and S 2s in Fe-sMoS_2 with weight loadings from 0% to 20%.

XPS spectra of Mo 3d and S 2s have been investigated and shown in Figure S16. It is interesting to find that with the introduction of Fe, both the peaks of Mo 3d and S 2s shift towards higher binding energy, indicative of the electronic donation from Mo and S to Fe, consistent with the result of XANES spectra. Thus, the S vacancies can enrich electron density of Mo but it cannot return to the original value by refilling the vacancies due to the strong electron donating to the Fe atoms by the sMoS_2 structure. We have added the above results and more discussions accordingly in the revised manuscript.

Figure S17. XPS spectra from Fe2p in Fe-sMoS_2 with weight loadings from 3% to 20%.

Fe(2p3/2) peak can be deconvoluted into two peaks as 710.5 eV and 712.4 eV, attributing to Fe(II) and Fe(III), respectively (Figure S17). Fe(II) is the main specie, consistent with the Fe k edge XANES study.

Figure S18. XPS survey spectrum of 10%Fe-sMoS_2.

Figure S19. Catalytic performance for RWGS over Fe-sMoS_2 and bulk MoS_2 at 10 bar, 300 °C and GHSV,= 9000 mL/g/h.

Figure S20. Catalytic performances of Fe-sMoS_2 with various Fe loading at different reaction temperatures. **a.** Conversion. **b.** Selectivity at 10 bar, GHSV= 9000 mL/g/h.

Figure S21. Catalytic stability over Fe-sMoS_2 at 10 bar, 300 ºC, GHSV= 9000 mL/g/h.

Figure S22. Catalytic stability over Fe-sMoS_2 at 1 bar, 300 °C, GHSV= 9000 mL/g/h.

Figure S23. k^3-weighted *R*-space Fourier transform spectra from EXAFS for 10%Fe-sMoS_2 after reaction in Figure S16.

Figure S24. Sulfur tolerance test over 10%Fe-sMoS_2 (300 °C) and Fe oxide on alumina (10 wt%) (450 °C) at 1 bar, GHSV= 9000 mL/g/h.

Figure S25. DRIFTS study for RWGS over $sMoS_2$ and 10%Fe-$sMoS_2$ at 300 ºC under CO_2 and H_2 (1:3), 30 min.

Table S1. ICP-OES data for the TMs loaded on $sMoS_2$.

TM species	Fe	Co	Ni	Cu	Pt	Pd	Ru
TM Loading (wt%)	9.34	9.58	10.31	9.44	8.93	9.16	9.08

Table S2. Fe content analysis based on ICP-OES and XPS for Fe-$sMoS_2$ at different wt% loadings.

Sample	Theoretical loading (wt%)	Loading from ICP-OES (wt%)	Loading from XPS (wt%)
3%Fe-$sMoS_2$	3.00	2.48	2.69
5%Fe-$sMoS_2$	5.00	4.28	4.51
10%Fe-$sMoS_2$	10.00	9.34	9.39
15%Fe-$sMoS_2$	15.00	12.33	12.92
20%Fe-$sMoS_2$	20.00	18.32	18.42

Table S3. Fitted coordination environment of Fe for EXAFS over Fe-$sMoS_2$ at different wt% loadings.

Sample	Scattering Path	Enot (eV)	R (Å)	CN	D-W factor	R factor (%)
3%Fe-$sMoS_2$	Fe-S	-6.19	2.216 ± 0.006	3.23	0.009 ± 0.001	0.60
5%Fe-$sMoS_2$	Fe-S	-4.22	2.231 ± 0.005	3.03	0.008 ± 0.001	0.83
10%Fe-$sMoS_2$	Fe-S	-1.26	2.238 ± 0.007	3.01	0.007 ± 0.001	1.26
15%Fe-$sMoS_2$	Fe-S1	-9.62	2.119 ± 0.024	1.99	0.005 ± 0.001	0.68
	Fe-S2	-9.62	2.286 ± 0.022	1.26	0.001 ± 0.003	
	Fe-Fe	9.37	2.993 ± 0.035	1.25	0.007 ± 0.002	
20%Fe-$sMoS_2$	Fe-S1	9.90	1.800 ± 0.012	1.99	0.011 ± 0.001	0.51
	Fe-S2	-9.90	2.374 ± 0.005	1.00	0.000 ± 0.005	
	Fe-Fe	-0.88	2.969 ± 0.035	2.18	0.008 ± 0.002	

"CN" is the coordination number; "D-W" is the Debye Waller (thermal atomic uncertainty); R is the bond length; Enot is the energy difference between theoretical and calculated scattering path.

Table S4. Elemental compositions and quantitative vacancy of Fe-sMoS_2 based on XPS analysis at different wt% loadings.

Sample	Atomic loading (%)			S/Mo	Vs (%)
	Fe	Mo	S		
MoS_2	0	33.99	66.01	1.94	3.5
sMoS_2	0	40.63	59.37	1.46	21.8
3%Fe-sMoS_2	2.7	38.60	58.70	1.52	18.5
5%Fe-sMoS_2	4.53	37.99	59.48	1.57	16.5
10%Fe-sMoS_2	9.42	34.03	56.55	1.66	11.5
15%Fe-sMoS_2	12.97	31.29	55.74	1.78	6.8
20%Fe-sMoS_2	18.49	28.53	52.98	1.86	4.1

"Vs" is the S vacancy content by [4*(the atomic ratio of Mo)-2*(the atomic ratio of S)]/2*100.

Supplementary Notes

Our main focus of this research is to address a reliable synthetic method for the preparation of high loading of metal on supports especially on the chalcogenide surface with the clear underlying principles for the strong anchoring interactions instead of claiming the recorded highest single atom loading in this work. Besides, many of the cited single atoms from the literature were not stable against aggregation under the conditions, not well characterised, no clear established molecular interactions in their complex systems and many times are unable to differentiate the roles of single atoms from clusters in catalysis, (i.e. the non-uniform dispersion and different types of N anchors and poorly defined gC_3N_4 rendered the authors unable to differentiate the atomic structures of Fe and clusters and the photo-Fenton reaction they used indicated that clusters may likely be more active than single atoms without knowing their precise bonding and structures.[5]

In this work, we present a new route to prepare metallic single atoms on chalcogenide at high loading by making use of their corresponding thiolcomplexes of defined structures for the preanchoring to the sulphur defects. The precise geometric locations, electronic interactions are clearly characterized with the atomic activity carefully monitored for the differentiation from clusters from the chosen RWGS reaction and the fundamental turnover frequency and stability can also be given without much controversy.

Fe is the only the benchmark of this work. As seen from the manuscript, the other transition metals including Cu, Co, Ni, Pt, Pd, Ru have also been deposited onto the $sMoS_2$ using the same method. A similar series of characterizations including XRD, STEM, EXAFS and ICP have been conducted, indicating the successful preparation of single atom supported chalcogenides.

However, the R&D on single atom catalysts may not have yet reached to the industrial practice. There are challenges in scale up and green synthesis aspects of our present method. As summarised by some latest reviews and articles, there is still an urgent need to prepare a reliable synthesis method for high loading of single atom on support with defined structure and interaction to allow the fundamental study for the specific reaction of interests in catalysis before industrial practice can be concluded. We believe that our present approach and materials can underpin further development in supported single atoms and their impacts in catalysis. See the details in the following,

1. Consideration of Green Aspects of The Synthetic Method

Concerning the green chemistry aspects of our method (with particular reference to the 12 principles of green chemistry: Green Chemistry: Theory and Practice Paul T. Anastas, John Charles Warner Oxford University Press, 1 Jan 2000), the present use of thiourea for the pre-formation of transition metal complexes, single molecular MoS_2 layer by n-BuLi and their reaction for the product synthesis is cumbersome, expensive, difficult to scale up and also is not green with a significant generation of wastes (Li containing wastes) at this stage. As a result, we have attempted to modify our method *without the pre-formation of thiourea* or N containing salt (potential NOx generation) but just using simple water soluble Fe salts for deposition on $sMoS_2$.

1) By using Fe acetate, it is found that Fe species can still be in atomic dispersed when the Fe loading is 3%. However, Fe clusters can be clearly formed when the loading is above 10%. These are confirmed by our EXAFS spectra in Figure S5b, only single characteristic peak is observed for 3%Fe-MoS_2-nt but two in 10%Fe-MoS_2-nt. Attempts to deposit simple Fe containing salts (i.e. Fe oxalate) by strong adhesion to the layer via defects without generation of wastes while maintaining the single Fe dispersion at wider loading should be tried for practical applications.

2) It is well known that the structure of transition metal dichalcogenides (TMDs) consists of sandwiched X-M-X (X=S, Se, Te, M=Mo, W, Ti, etc.) molecular layers including MoS_2, which are held by weak van der Waals interaction, similar to graphite. This weak interaction allows the preparation of 2-D nanosheets in solution through a number of top-down exfoliation methods of bulk crystals. Physical or mechanical cleavage by a scotch-tape method can be used to extract high quality mono- or few- layered TMDs but this method is difficult to scale up for mass production.

Here we used n-BuLi method for initial demonstration, which is well accepted method for exfoliation. However such chemical method is synthetically cumbersome and the materials are highly sensitive to operating conditions and can generate significant wastes. Recently a direct liquid exfoliation method with ultrasonic treatment has also been demonstrated to show enormous potentials in mass scale production to meet industrial requirements. For example, Coleman and co-workers employed this method to exfoliate LMs to nanosheets efficiently in a selected solvent with appropriate Hansen solubility parameters.[6] Such physical separation method can demonstrate an aesthetic appeal due to its simplicity and ease of handling without any chemical reaction involved.

As a result, we attempted a related solvent method[7] prior to Fe loading, it was found that the exfoliated MoS_2 can carry 3% Fe single atoms but increasing the loading to 10% causes the aggregation of Fe species on the sample. However, we feel that for potential green synthesis, using mixed solvents guided by Coleman method should be more seriously attempted in a relatively greener way to prepare single atom chalcogenide layer.

2. Sulfur Tolerance

RWG catalyst with higher degree of sulfur tolerance is one of the main drivers for the investigation of sulphide based catalysts in this area. We have tested the effect of introduction of thiophene (~100 ppm) into the CO_2/H_2 mixture over this highly dispersed Fe-$sMoS_2$ as to compare with Fe oxide catalyst. As seen, the former clearly shows a stronger sulfur tolerance than the latter, presumably the synergetic CO_2/H_2 activation to maintain activity over this Fe/$sMoS_2$ showing the potential applications of this catalyst (Figure S24).

Reference

1. Liu, G.; Robertson, A. W.; Li, M. M.-J.; Kuo, W. C. H.; Darby, M. T.; Muhieddine, M. H.; Lin, Y.-C.; Suenaga, K.; Stamatakis, M.; Warner, J. H.; Tsang, S. C. E. MoS_2 Monolayer Catalyst Doped with Isolated Co Atoms for the Hydrodeoxygenation Reaction. *Nat. Chem.* **2017**, *9* (8), 810–816.
2. Kresse, G.; Furthmuller, J. Efficient Iterative Schemes for Ab Initio Total-Energy Calculations Using a Plane-Wave Basis Set. *Phys. Rev. B: Condens. Matter Mater. Phys*. **1996**, *54*, 11169–11186.
3. Kresse, G.; Joubert, D. From Ultrasoft Pseudopotentials to The Projector Augmented-Wave Method. *Phys. Rev. B: Condens. Matter Mater. Phys*. **1999**, *59*, 1758–1775.
4. Perdew, J. P.; Chevary, J. A.; Vosko, S. H.; Jackson, K. A.; Pederson, M. R.; Singh, D. J.; Fiolhais, C. Atoms, Molecules, Solids, and Surface: Applications of The Generalized Gradient Approximation for Exchange and Correlation. *Phys. Rev. B: Condens. Matter Mater. Phys.* **1992**, *46*, 6671–6687.
5. An, S.; Zhang, G.; Wang, T.; Zhang, W.; Li, K.; Song, C.; Miller, J. T.; Miao, S.; Wang, J.; Guo, X. High-density ultra-small clusters and single-atom Fe sites embedded in graphitic carbon nitride (g-C3N4) for highly efficient catalytic advanced oxidation processes. *ACS nano* **2018,** *12* (9), 9441–9450.
6. Coleman, J. N.; Lotya, M.; O'Neill, A.; Bergin, S. D.; King, P. J.; Khan, U.; Young, K.; Gaucher, A.; De, S.; Smith, R. J.; Shvets, I.V. Two-dimensional nanosheets produced by liquid exfoliation of layered materials. *Science* **2011** *331* (6017) 568–571.
7. Liu, G.; Ma, H.; Teixeira, I.; Sun, Z.; Xia, Q.; Hong, X.; Tsang, S. C. E. Hydrazine-assisted liquid exfoliation of MoS_2 for catalytic hydrodeoxygenation of 4-methylphenol. *Chem. Eur. J.* **2016** *22* (9) 2910–2914.